26th IMEKO TC4 International Symposium
24th International Workshop on ADC and DAC Modelling and Testing
IMEKO TC-4 2023
Pordenone, Italy / September 20-21, 2023

Quantum magnetometry with OPM: Novel applications in non-destructive testing?

Andreas Blug[1], Kerstin Thiemann[1], Simon Philipp[2], Thomas Straub[2], Alexander Bertz[1]

[1] *Fraunhofer Institute for Physical Measurement Techniques IPM, Freiburg, Germany.*
E-mail: prename.name@ipm.fraunhofer.de, e.g., andreas.blug@ipm.fraunhofer.de
[2] *Fraunhofer Institute for Mechanics of Materials IWM, Freiburg, Germany*
E-mail: prename.name@iwm.fraunhofer.de

Abstract **– Microfabricated optically pumped magnetometers (OPM) are a novel class of commercially available quantum magnetometers combining high sensitivity with high dynamic range. In non-destructive testing (NDT) this should enable new applications like measuring stray fields arising from small stress concentrations affecting local magnetization. In ferromagnetic steel the sensitivity of OPM is sufficient to measure magnetization from critical stresses for crack initiation in submillimeter volumes. However, OPM, as they are built today, require additional components like magnetic flux guides to control the measurement volume in NDT systems. The improvement of spatial resolution with such a flux guide is demonstrated using neighbored weld seams as an example for stress concentrations.**

I. INTRODUCTION

Quantum magnetometers like OPM exploit fundamental physical constants so that no calibration is required and quantum techniques as entanglement or spin squeezing to achieve a higher statistical precision than classical approaches [1, 2]. This results in robust and highly sensitive devices with extraordinary dynamic range close to the physical limits [3]. OPM measuring magnetic fields by their interactions between resonant light and atomic vapor have evolved rapidly during the past two decades. Modern ones, as they became commercially available in recent years, are microfabricated systems consisting of one or more small vapor cells (~ 1 mm³) of gaseous helium or alkali atoms that are pumped by a laser to spin states similar to atomic clocks [4-7]. They measure spins collectively precessing around the magnetic field direction with the so-called Larmor frequency. Depending on the read-out mechanism, different sensitivities and measurement ranges are achieved. Table 1 lists specifications of some commercially available OPM sensors which might be interesting for applications in the field of non-destructive testing (NDT). They achieve similar sensitivities as superconducting quantum interference devices (SQUIDs), but without complex and expensive cryogenic cooling.

Table 1. Some commercially available OPM sensors.

	Fieldline V3 [8]	Mag4Health He-4-mag. [9]	QuSpin total-field mag. [10]
Gas	Rb	^{4}He	Rb
B-field	single axis	vector xyz	scalar
Sensitivity	15 fT/√Hz	40 fT/√Hz	3 pT/√Hz
Dyn. range	50 nT	250 nT	100 µT
Bandwidth	250 Hz	2 kHz	500 Hz
Size [mm³]	13x15x36	20x20x50	12x18x36

As passive magnetic NDT methods like “metal magnetic memory” (MMM) measure local variations of magnetization due to stress or microscopic structure within a volume in ferromagnetic materials, OPM are beneficial to decrease that measurement volume [11-13], i.e., to increase either lateral resolution for stress concentration measurement or depth resolution for structural changes like martensite-austenite transitions in hardening layers. The major challenges for using these systems are to control the measurement volume and to suppress ambient perturbations from microtesla to picotesla scale. A particular benefit would be to measure stress concentrations with a submillimeter resolution because such stress concentrations are the precondition for crack initiation [14, 15].

II. PIEZOMAGNETIC FATIGUE TESTING

A first setup to learn about the evolution of magnetic signals over the lifetime of a material is shown in Fig. 1. It combines a cyclic fatigue setup with a OPM in a shielded environment. As shown in Fig. 1a, the specimen is mounted on ceramic rods where the right end is moved by a piezo actor and the left is connected to a force measurement cell. The zero-field OPM measures the vertical component of the magnetic stray field B varying with force F and strain ε [16]. The coils on the inner layer of the magnetic shield control the magnetic environment

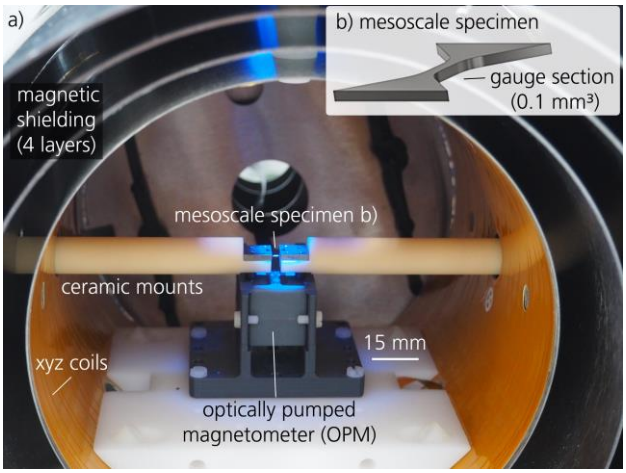

Fig. 1. a) Setup for piezomagnetic fatigue testing with mesoscale specimen (b). Magnetic signals arise from the gauge section with a volume of 0.6x0.4x0.4 mm³.

of both, specimen and OPM sensor. In contrast to similar experiments with classical magnetometers [17, 18], the gauge section of the specimen can where fatigue damage accumulates can be decreased from cm to sub-mm scale which makes it much easier to link events in the magnetic signal to metallographic characterizations. The noise within the shielding is below 1 pT at a measurement rate of 100 Hz, even if the sample is moved.

Fig. 2 shows the evolution of the mechanical hysteresis (F-ε) and of the piezomagnetic hysteresis (B-ε) over the lifetime of a ferritic steel specimen. A 5%-drop of force amplitude is used as end-of-life criterion [19]. The complete signals over the lifetime of 140 cycles are drawn light grey; some of them are colored to illustrate the evolution. Up to that point, microscopic defects like dislocations, grain boundaries, precipitates, and non-magnetic inclusions are accumulated in the material without crack initiation and the stiffness of the sample is not altered significantly. Therefore, force F hardly changes apart from some hardening in the beginning. In the piezomagnetic curve, two major effects are visible: firstly, the major change in magnetic stray field B occurs in the elastic parts of the mechanical hysteresis, i.e., the steep slopes in the mechanical hysteresis (F-ε). This corresponds to the stress response of magnetization of the material [20]. Secondly, the amplitude of the piezomagnetic hysteresis varies much stronger over the lifetime than the force signal due to pinning effects between fatigue damage and magnetic domain walls.

For NDT applications, these experiments demonstrate that OPM can resolve the variation of the magnetic stray field corresponding to yield condition in a volume of 0.1 mm³, i.e., on a submillimeter scale. The amplitude of the magnetic stray field varies by about 5 nT between positive and negative yield stress. However, the lateral resolution is defined by the distance between the vapor cell

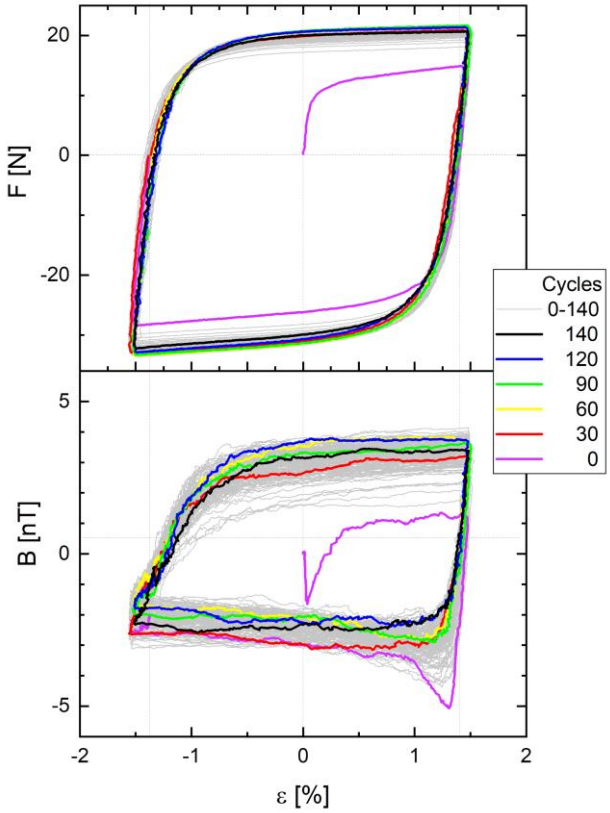

Fig. 2. Piezomagnetic fatigue signals for a ferritic steel specimen. End-of-life criterion is a 5% drop of force. Mechanical hysteresis (F-ε) of force F and strain ε, and piezomagnetic hysteresis (B-ε) of magnetic stray field B and strain ε.

inside the sensor, where the magnetic field is measured, and the specimen surface. In the setup of Fig. 1 it is about 12 mm – the minimum distance between vapor cell and sensor surface is about 6 mm. Therefore, additional components like pick-up coils or flux guides are required to control the measurement volume.

III. SPATIAL RESOLUTION AT WELD SEAMS

To confine the measurement volume, Kim and Savukov used flux guides from Mn-based ferrites to measure the lateral component of the magnetic field with high spatial resolution of 0.25 mm [21]. For the setup in Fig 3a, we use a different flux guide geometry measuring the normal component of the external magnetic field [22]. This geometry should be appropriate for NDT of ferromagnetic specimen as their inner magnetic field is refracted towards the normal at the surface due to their high magnetic permeability μ_r. The setup in Fig 3a uses a similar shielding as the fatigue trials Fig. 1. The zero-field OPM is embedded in a 3D printed structure holding a flux guide with a conically shaped tip.

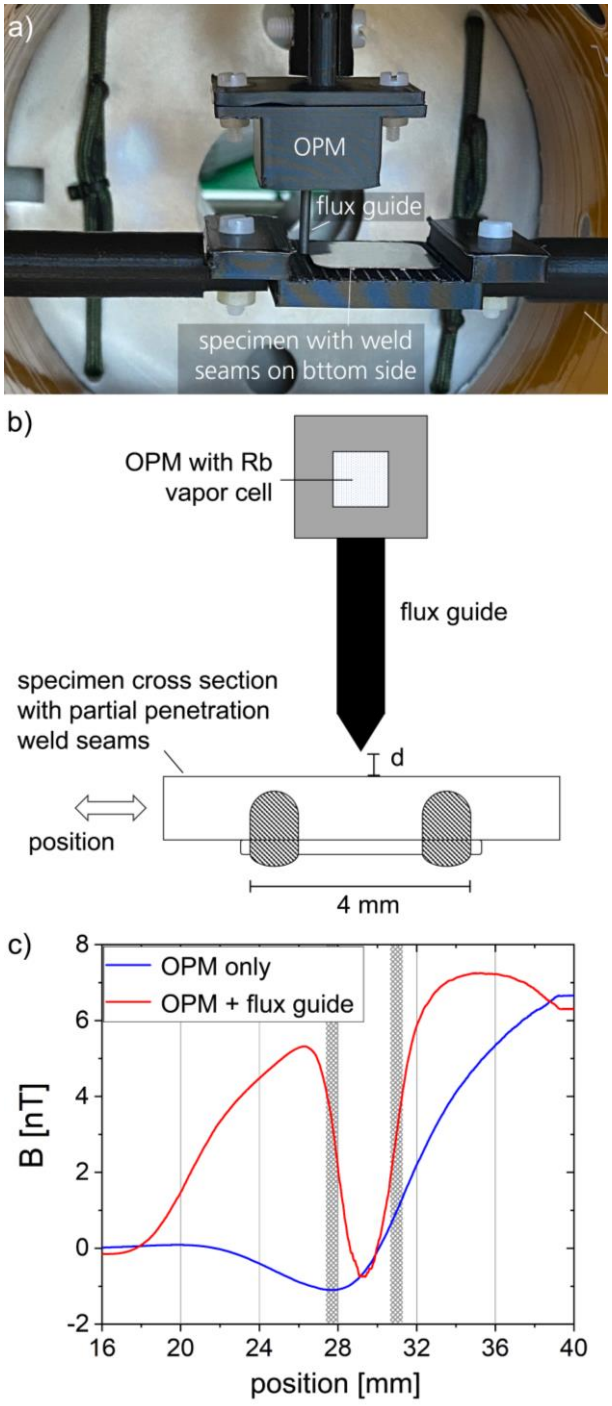

Fig. 3. Detection of two partial penetration weld seams separated by 4 mm. A): image of the setup with OPM, flux guide and specimen. B) sketch of OPM with Rb vapor cell, flux guide, and cross section of a moving specimen with weld seams. C) distribution of magnetic stray field B measured with (red) and without flux guide (blue).

To demonstrate the improvement of spatial resolution, a steel sample with two neighbored partial penetration weld seams serving as localized stress concentrations due to thermal expansion [23 - 25]. As sketched in Fig. 3b, the weld seams are separated by 4 mm, attaching a second layer of ferromagnetic steel. No heat affected zone is visible on the bottom of the sample so that the distance d between sample and tip of the flux guide remains constant when the sample is moved. The diameter of the flux guide is 1.5 mm.

The comparison between the measurements with the OPM sensor only guided close to the sample (blue) and the combination of OPM and flux guide (red) is shown in Fig. 3. In both cases, the distance d between sample surface and OPM housing in the first case and flux guide in the second case is estimated visually to about 1 mm. The sample has a magnetic gradient across the scanned line. However, the expected pairwise symmetry of the weld seams is only visible in the magnetic signal acquired with flux guide. Due to the flux guide, the noise level rises from 0.5 to 2 pT, but with increased lateral resolution in the range of about 2 mm at the depth of the weld seam. By further optimizing the flux guide geometry, it should be possible to achieve sub-millimeter spatial resolution in this configuration.

IV. DISCUSSION

Microfabricated optically pumped magnetometers (OPM) are among the first commercially available quantum sensors. Total-field OPM have an exceptional dynamic range with a sensitivity of 3 pT/√Hz in an environment of 100 µT, i.e., in earth magnetic field. Zero-field OPM based on Rb or He vapor cells achieve sensitivities below 100 fT/√Hz – similar to SQUIDs, but without cryogenic cooling which simplifies high-sensitive magnetometry systems enormously. Due to these properties, OPM sensors open new applications in magnetic NDT.

In the piezomagnetic fatigue experiments, the magnetic stray field from a volume of only 0.1 mm³ varying by 5 nT is measured at a specimen from ferritic steel. The magnetic signal is much more sensitive to the accumulation of damage in the sample's gauge area than the stress-strain signal, which is a first step towards a magnetic fingerprint for mechanical degradation. The noise level of 0.5 pT without and of 2 pT with flux guide is also sufficient to measure critical stress concentrations arising from weld seams or material defects as precondition for crack initiation. Here, a flux guide is required to confine the measurement volume so that residual stresses of two neighbored weld seams separated by 4 mm could be resolved. With some optimization, sub-millimeter resolution appears feasible.

To test ferromagnetic devices in industrial environments, key components like flux guides, shielding, and low-stray-field actuators must be developed. Doing

that, the result can be a new generation of non-destructive testing systems estimating the remaining lifetime in maintenance or in the production if higher levels of functional safety are required or to assess the quality of critical weld seams.

ACKNOWLEDGEMENTS

This work was supported as a Fraunhofer LIGHTHOUSE PROJECT (QMag). We acknowledge financial support from the Ministry of Economic Affairs, Labor and Housing of the State of Baden-Württemberg, Germany. Thanks also to Ralph Sperling from Fraunhofer IMM for manufacturing the flux guides.

REFERENCES

[1] D. Budker, M. Romalis, “Optical magnetometry,” nature physics, vol. 3, pp. 227–234, 2007.

[2] L. Pezzè, A. Smerzi, M. K. Oberthaler, R. Schmied, P. Treutlein, “Quantum metrology with nonclassical states of atomic ensembles,” Rev. Mod. Phys., vol. 90, no. 3, p. 99, 2018.

[3] M. W. Mitchell, S. Palacios Alvarez, “Colloquium: Quantum limits to the energy resolution of magnetic field sensors,” Rev. Mod. Phys., vol. 92, no. 2, 2020.

[4] S. Knappe, O. Alem, D. Sheng, J. Kitching, “Microfabricated Optically-Pumped Magnetometers for Biomagnetic Applications,” J. Phys.: Conf. Ser., vol. 723, p. 12055, 2016.

[5] V. Shah et al., “Fully integrated, standalone zero field optically pumped magnetometer for biomagnetism,” Proc. SPIE 10548, p. 51, 2018.

[6] F. Bertrand et al., “A 4He vector zero-field optically pumped magnetometer operated in the Earth-field,” The Review of scientific instruments, vol. 92, no. 10, p. 105005, 2021.

[7] N. V. Nardelli, A. R. Perry, S. P. Krzyzewski, S. A. Knappe, “A conformal array of microfabricated optically-pumped first-order gradiometers for magnetoencephalography,” EPJ Quantum Technol., vol. 7, no. 1, p. 664, 2020.

[8] HEDscan V3 spec sheet, Fieldline Inc., 4845 Sterling Drive, 200, Boulder CO 80301, USA. https://fieldlineinc.com/ (accessed: Mar. 30, 2023)

[9] Mag4Health SAS, 9 Avenue Paul Verlaine, 38100 Grenoble, F, He-4 magnetometer. [Online]. https://www.mag4health.com/product/ (accessed: Mar. 23, 2023).

[10] QuSpin, Inc., 331 South 104th Street, Louisville, CO 80027, Quspin QTFM Gen-2. [Online]. https://quspin.com/qtfm-gen-2/ (accessed: Mar. 23, 2023).

[11] Z. D. Wang, Y. Gu, Y. S. Wang, “A review of three magnetic NDT technologies,” Journal of Magnetism and Magnetic Materials, vol. 324, no. 4, pp. 382–388, 2012.

[12] M. Roskosz, M. Bieniek, “Evaluation of residual stress in ferromagnetic steels based on residual magnetic field measurements,” NDT & E International, vol. 45, no. 1, pp. 55–62, 2012.

[13] N. Sonntag, B. Skrotzki, R. Stegemann, P. Löwe, M. Kreutzbruck, “The Role of Surface Topography on Deformation-Induced Magnetization under Inhomogeneous Elastic-Plastic Deformation,” Materials (Basel, Switzerland), vol. 11, no. 9, 2018.

[14] S. Gustafson et al., “Quantifying microscale drivers for fatigue failure via coupled synchrotron X-ray characterization and simulations,” Nature communications, vol. 11, no. 1, p. 3189, 2020.

[15] P. Ferro, “The local strain energy density approach applied to pre-stressed components subjected to cyclic load,” Fatigue Fract Engng Mater Struct, vol. 37, no. 11, pp. 1268–1280, 2014.

[16] P. A. Koss et al., “Optically Pumped Magnetometer Measuring Fatigue-Induced Damage in Steel,” Applied Sciences, vol. 12, no. 3, p. 1329, 2022, doi: 10.3390/app12031329.

[17] A. Ouaddi et al., “Passive piezomagnetic monitoring of structures subjected to in-service cyclic loading: Application to the detection of fatigue crack initiation and propagation,” AIP Advances, vol. 11, no. 1, p. 15344, 2021.

[18] S. Bao, T. Erber, S. A. Guralnick, W. L. Jin, “Fatigue, Magnetic and Mechanical Hysteresis,” Strain, vol. 47, no. 4, pp. 372–381, 2011.

[19] K. Thiemann et al. "Using optically pumped magnetometers to identify initial damage in bulk material during fatigue testing." Quantum Technologies 2022. Vol. 12133. SPIE, 2022.

[20] D. C. Jiles, “Theory of the magnetomechanical effect,” J. Phys. D: Appl. Phys, no. 28, p. 1537, 1995.

[21] Y. J. Kim, I. Savukov, “Ultra-sensitive Magnetic Microscopy with an Optically Pumped Magnetometer,” Scientific reports, vol. 6, p. 24773, 2016.

[22] U. Poppe et al., “High temperature superconductor dc-SQUID microscope with a soft magnetic flux guide,“ Jpn. J. Appl. Phys. 17(5), S191-S195 (2004).

[23] R. Stegemann et al., “Influence of the Microstructure on Magnetic Stray Fields of Low-Carbon Steel Welds,“ J Nondestruct Eval 37(3), 1821 (2018).

[24] F. Giudice, A. Sili, “A theoretical approach to the residual stress assessment based on thermal field evaluation in laser beam welding,” Int J Adv Manuf Technol, vol. 123, 7-8, pp. 2793–2808, 2022.

[25] A. Blug et al., “The full penetration hole as a stochastic process: controlling penetration depth in keyhole laser-welding processes,” Appl. Phys. B, vol. 108, no. 1, pp. 97–107, 2012.